INFLUENCE OF COUPLED DEFORMATION-DIFFUSION EFFECTS ON THE RETARDATION OF HYDRAULIC FRACTURE

by

Andy L. Ruina*

Division of Engineering

Brown University

May 1978

*Research Assistant in Engineering, Brown University

National Science Foundation Energy Trainee.

Preface

This report consists of two parts.

The first part is the text of the paper "Influence of Coupled Deformation-Diffusion Effects on the Retardation of Hydraulic Fracture" published in the Preprint-Proceedings of the 19th U.S. Symposium on Rock Mechanics held at Stateline, Nevada, May 1-3, 1978, compiled by Yung Sam Kim, published by C.I.E.P.C.E. University of Nevada-Reno, 1978, pp. 274-282. This first part (pp. 1-9) contains the Abstract, discussion of the Physical problem, basic aspects of the mathematical model, highlights of the solution and discussion of the results.

The second part (pp. 10-41) contains the details of the mathematical analysis and solution and may be regarded as a collection of unpublished appendices to the first part of the paper.

The body of the report has been submitted as the thesis "Steady State Growth of a Mode I Fracture in a Fluid Saturated Porous Elastic Material," June 1978 in partial fulfillment of the requirements for an Sc.M. degree in Engineering (Solid Mechanics) at Brown University.

TABLE OF CONTENTS

APPENDICES

INFLUENCE OF COUPLED DEFORMATION-DIFFUSION EFFECTS ON THE RETARDATION OF HYDRAULIC FRACTURE.

INFLUENCE DES EFFETS COUPLES DEFORMATION-DIFFUSION SUR LE RETARD DE LA FRACTURE HYDRAULIQUE.

EINFLUSS VON GEKUPPELTEN DEFORMATIONS-DIFUSIONS EFFEKTEN AUF DAS HYDRAULISCHE BRUCHVERHALTEN.

by Andy Ruina
Graduate Research Assistant
Brown University
Dept. of Engineering, Box D
Providence, R.I. 02912 USA

ABSTRACT

Hydraulic fracture of a saturated porous rock formation is discussed, taking into account the full coupling between matrix deformation and ambient pore fluid diffusion. In order to isolate the porous-media effects and simplify the formulation, we consider the growth of a semi-infinite, plane-strain, mode I crack at constant speed, v. The matrix is modeled by the equations governing quasi-static deformation of a porous, fluid-saturated, isotropic, linear elastic medium as expressed by Rice and Cleary [12]. The two porous media effects slowing the growth of hydraulic fracture discussed here are: (i) the decrease in the stress singularity at the crack tip with increased speed of crack advance; (ii) the decrease in pore fluid pressure near the crack tip with increasing crack propagation speed (causing a decrease in the Terzaghi effective tension stress). The magnitudes of these effects and the speeds at which they become important are found by solving (or partially solving) the porous media equations for two different applied loadings. General results are found analytically and some detailed results are obtained numerically. The full stress and pore pressure fields are found near the crack tip for fast propagation speeds.

Glossary

B	pore pressure coefficient, dimensionless
c	diffusivity, [length]^2[time]$^{-1}$ = [ℓ]^2[t]$^{-1}$
e	2.71828 ... (base of natural log)
f_{ij}	functions describing crack tip stress field
g	gravitational constant [ℓ][t]$^{-2}$
i,	coordinate axis label, $(-1)^{\frac{1}{2}}$
j,	coordinate axis label
K,	stress intensity factor [force][ℓ]$^{-3/2}$
ℓ,	crack length
p,	excess pore fluid pressure [force][ℓ]$^{-2}$
q,	mass flux rate of pore fluid [m][ℓ]$^{-2}$[t]$^{-1}$
r,	distance from crack tip
v,	crack tip propagation speed
x,y	coordinate axes
β	$(1-\nu)/(1-\nu_u)$ - see below
θ	angle from positive x axis
κ	pore fluid permeability [ℓ]^3[t][m]$^{-1}$
λ	crack face loading wave number [ℓ]$^{-1}$
ρ	pore fluid density
σ	total stress, [force][ℓ]$^{-2}$
τ	crack face loading, [force][ℓ]$^{-2}$
ν,ν_u	drained, undrained Poisson's ratio, dimensionless
ω	length of crack tip decohesion zone

INTRODUCTION

Hydraulic fracture is the generic term for the initiation and propagation of underground cracks caused by the injection of a 'fracturing' fluid at high pressure. Applications of hydraulic fracture include [8,9,14]: 1) the opening of short or long fissures adjacent to oil or gas wells to increase the surface area or the range of the well, 2) aiding underground waste disposal, 3) creation of an underground network in hot rock for geothermal energy recovery, 4) determination of underground (tectonic) stress by means of monitoring the initiation and growth of hydraulic fractures.

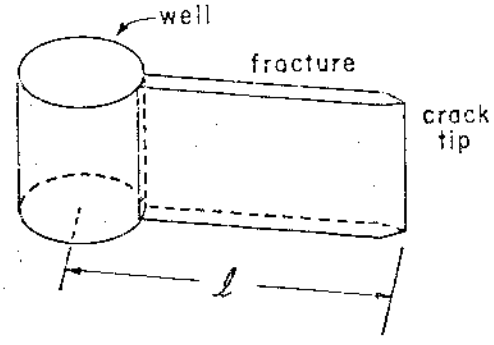

FIGURE 1; Approximate geometry of typical hydraulic fracture. Fracturing fluid is pumped into the well, which is plugged above and below the region shown, causing the inception and growth of fracture.

Hydraulic fracture also has been suggested as part of the mechanism in the Teton dam collapse [16].

The general process of hydraulic fracture is as pictured (in a geometrically idealized form) in figure 1. A fracturing fluid (not to be confused with ambient pore fluid) is pumped into a region of a well that is plugged at the top and bottom (the plugs are above and below the section of well shown in the figure). The tensile stress tangent to the well perimeter (hoop stress) increases to the point of crack initiation at which time the measured pressure of the fracturing fluid generally drops suddenly and then recovers to a fairly constant level as more fluid is pumped into the extending, often vertical crack.

The fracturing fluid is often very viscous, so as to facilitate the transport of sand or some other propping agent into the crack, and to minimize the loss of fracturing fluid through the crack faces.

A full understanding of the growth of a hydraulic fracture involves knowledge of the progressive shape of the fracture and an understanding of the fluid dynamics within the crack (and into the crack faces) as coupled with the deformation of the surrounding medium and resultant crack growth. The complexity of the problem requires that analytical studies be highly idealized and focused on particular effects.

Of particular interest is the determination of conditions under which the fracture will extend and the determination of the extent of crack growth from records of the fracturing fluid pressure and rate of pumping.

Nordgren [11] calculated the progressive length of a vertical fracture with fixed height (small compared to the length). In Nordgren's model viscous losses between the crack faces, and fluid loss into the formation are the factors that control crack growth.

Geertsma and deKlerk [6] analyze both a horizontal penny-shaped fracture and a vertical fracture (with length small compared to height). In their model the fracture is retarded by the above effects as well as a strong closure stress in the crack tip region caused by an assumed lack of penetration of fracturing fluid there. Both of the above studies neglect the fracture toughness (and tensile strength) of the rock.

The fracture toughness of the rock has been accounted for in more recent work for the case of a penny-shaped fracture (Abe et al., [1]) and for a vertical fracture with large height (Mahmoud and Clifton [10]). In all of the above studies the fractured formation has been modelled as isotropic, homogeneous and linear elastic.

The fractured formation is in fact frequently porous. The formation porosity is accounted for in some of the above references by the leakage of fracturing fluid into the formation. Haimson et al. [7], Geertsma [5], (and a review by Friedman [4]) consider alterations in stress near the well bore due to the penetration of fracturing fluid around the well hole. Fracture initiation is determined by the effective stress, $\sigma_{\theta\theta} + p$ ($\sigma_{\theta\theta}$ is the tensile hoop stress) in their model, where the pore pressure is altered by the penetration of the fracturing fluid. Geertsma [5] briefly considers the effects of fracture fluid permeating the fracture surfaces during crack extension. He finds that the strains

induced by the fracturing fluid pressure in the pore space have little effect on fracture.

Cleary [2,3] has taken into account the full consolidation-like coupling between deformation of the fluid-saturated solid matrix and diffusive motions of the ambient pore fluid. This coupling results in a time dependent response in the formation, in contrast to all of the above studies, which only include rate effects due to the motion of fracturing fluid between and into the crack faces. Cleary used the Biot three dimensional consolidation equations and known plane strain dislocation solutions [12] of these equations. He represented hydraulic fractures and shear faults by a superposition of appropriate dislocations and numerically solved the resulting integral equations. Cleary's solutions demonstrate that both hydraulic (mode I) and shear (mode II) fractures require increased imposed loads to propagate at increased, quasi-static (dynamic terms neglected) speeds.

Rice and Simons [13] and Simons [18] verified and improved Cleary's results for shear faults by using analytical methods. The present paper treats the hydraulic fracture in a manner analogous to the works just mentioned [13,18] and confirms Cleary's overall findings. The solutions given here also provide a more complete description of the crack tip stress and pore pressure fields.

BASIC ASPECTS OF THE MODEL

The fracture is assumed to be vertical and all field variables are assumed to vary negligibly with height. The calculations are thus plane strain in the x,y plane of figure 2. After crack initiation the fracture of figure 1 is easily pictured to be well approximated by the flat crack of figure 2a. The equations to be used are linear and thus superposition can be used as is indicated in figure 2a where the compressive stress $\sigma^{ambient}$ is the tectonic stress normal to the crack face and $\tau(x)$ is the net loading on the crack faces and is given by $\tau(x)$ = (actual crack face load) - $\sigma^{ambient}$. In ordinary linear elasticity the crack tip fields resulting from constant load on a finite crack are very close to the fields due to constant loading over a finite length on a semi-infinite crack [13,19]. This justifies the approximation of 2b, at least for general results or results relating to behavior very near the crack tip.

In order to isolate the porous media effects and simplify the formulation all coupling between displacement of the crack walls and the pressure distribution in the fracturing fluid is ignored (see earlier references for discussion of these effects [1,4,5,6,7,10,11]).

The mathematics and formulation are further simplified by eliminating time as an independent variable. This is done by assuming that the crack tip advances at a constant speed v and that all field variables do not vary in time relative to an observer who moves with the crack tip. Thus, relative to the crack tip the problem is "steady state." The "steady state" assumption is obviously a great idealization in a process as unsteady as hydraulic fracture. Nonetheless, the solutions generated should be representative of the consequences of the effects being discussed even for unsteady v. Also, some of the high speed results calculated for constant v may be directly applicable to unsteady v [15].

Specification of the crack face loading $\tau(x)$, and the speed of crack growth v, with assumptions about material properties is enough (in principle) to solve for the complete stress and strain fields. In

our model the values of all field variables depend linearly on the intensity of the loading and in a manner to be shown, on v. However, in the physical problem the crack face loading and the speed of crack propagation, v, are not independent variables. If crack advance is considered to depend on attaining a critical level of some property of the stress or strain fields near the crack tip, then the required magnitude of loading for any given velocity can be determined. The central subject of this paper is the relationship between crack tip velocity and the magnitude of the required loading.

Criterion for Crack Extension

Two different models are used to determine the critical level of the stress and strain field for crack growth. The first is based on the critical stress intensity factor $K_{crit.}$ of fracture mechanics. In linear elasticity, with no pore fluid effects, the stress field near a sharp crack tip is dominated by a term of the form

$$\sigma_{ij}^{elastic} = Kf_{ij}(\theta)/(2\pi r)^{\frac{1}{2}} \qquad (1)$$

where r is the distance from the crack tip; K, the stress intensity factor, is dependent on the location and strength of the external loads; and the functions f_{ij}, normalized so $f_{yy}(0) = 1$, are independent of the loading (assumed symmetric about the x-axis). The stress intensity factor K is thus a single parameter which characterizes the near tip stress field. The magnitude of any critical near-tip stresses or strains are proportional to K, hence the use of $K = K_{crit.}$ as a crack extension criterion.

In our case, with a fluid-infiltrated elastic solid, it will again be found that the near crack tip stress field has the form

$$\sigma_{ij}^{porous\ elastic} = Kf_{ij}(\theta)/(2\pi r)^{\frac{1}{2}} \qquad (2)$$

so long as r is sufficiently small, although K will now also depend on v; in fact, as it turns

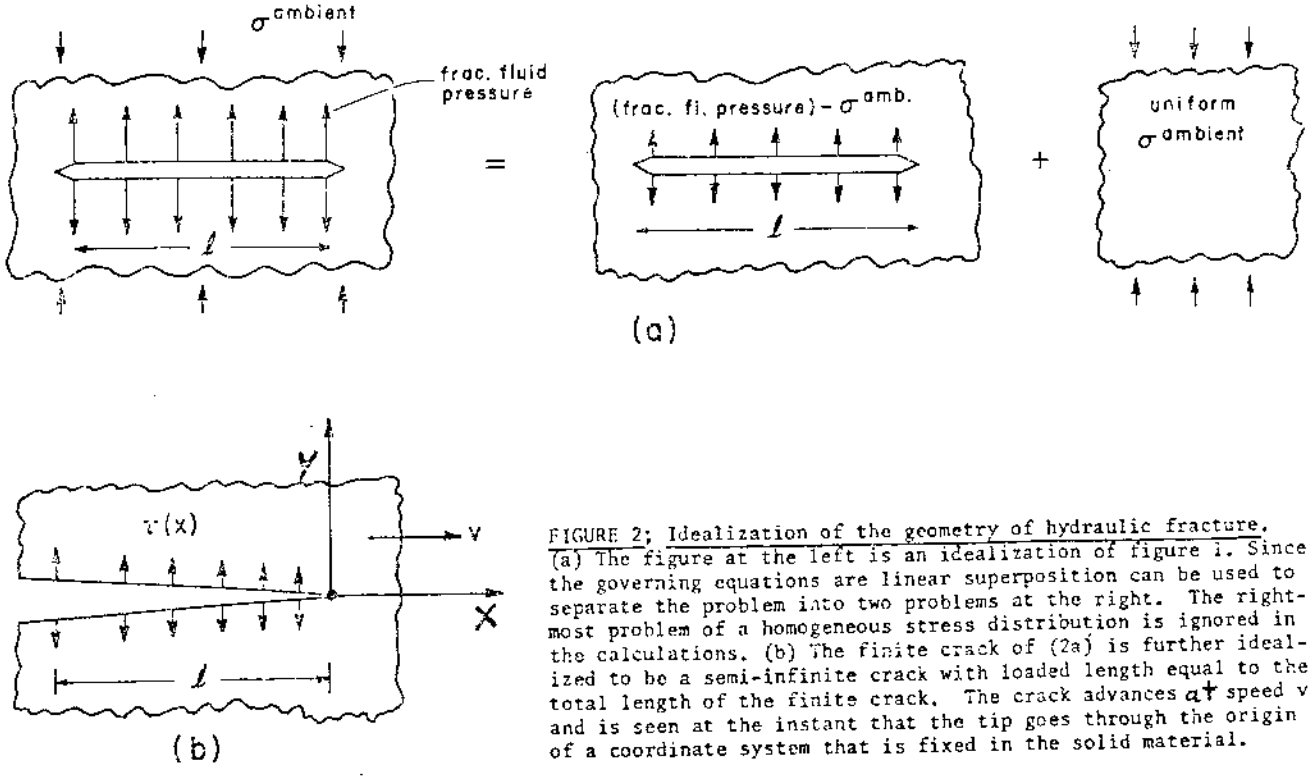

FIGURE 2; Idealization of the geometry of hydraulic fracture. (a) The figure at the left is an idealization of figure 1. Since the governing equations are linear superposition can be used to separate the problem into two problems at the right. The rightmost problem of a homogeneous stress distribution is ignored in the calculations. (b) The finite crack of (2a) is further idealized to be a semi-infinite crack with loaded length equal to the total length of the finite crack. The crack advances at speed v and is seen at the instant that the tip goes through the origin of a coordinate system that is fixed in the solid material.

out, it is smaller, for $v > 0$, than the K the same loads would cause on an ordinary elastic material. Thus the $K_{crit.}$ concept can still be used, provided the actual material breakdown process happens close enough to the crack tip so that eq. (2) is valid. As will be seen, within this range of r the excess pore pressure p is zero, and so the effective stress $\bar{\sigma}_y \equiv \sigma_y + p$ is the same as the total stress. (In cases where tectonic stresses and ambient pore pressures are present, all variables represent the excesses of quantities above their ambient values). For large v it is possible, as will be shown, that the physical breakdown process occurs outside the domain of eq. (2) and another fracture criterion is required. The effective stress criterion, $\bar{\sigma}_y(\omega) = \bar{\sigma}_{crit.}$, is used here where ω is a distance representing the size of the material breakdown zone at the crack tip and $\bar{\sigma}_{crit.}$ is a representative effective tensile stress required for failure. This criterion is the simplest that incorporates the facts that 1) rock failure depends on the effective stress [9]; 2) decohesion at the crack tip takes place over a finite distance. This model is intended to replace physically more realistic but computationally more difficult models [2,13]. When the loads and crack propagation velocity are such that the near tip effective stress field is fully described by (2) over a range of r that includes ω, this fracture criterion and $K = K_{crit.}$ are equivalent, provided that $K_{crit.}$ and $\bar{\sigma}_{crit.}$ are related by $K_{crit.} = \bar{\sigma}_{crit.} (2\pi\omega)^{\frac{1}{2}}$. This is true in a very slowly growing crack where all excess pore pressure is fully drained.

Field Equations

Rice and Cleary's [12] form of Biot's constitutive equations for linear, isotropic, elastic, fluid infiltrated (with linear pore pressure effects) porous media is used here. The equations can be derived from Darcy's law, linearity, isotropy and the existence of an internal energy density [15]. The isotropic form of Darcy's law used is:

$$q_i = -\rho_o \kappa \partial p/\partial x_i \qquad i=1,2,3 \qquad (3)$$

where q_i is the mass flux rate of pore fluid in the x_i direction, κ is the permeability, ρ_o is the fluid density and p is the excess pore pressure. The permeability is measured variously in units of length squared [9] $\mu\kappa$, where μ is the pore fluid viscosity, or in units of length per second [20] $\rho g \kappa$, where g is the local gravitational constant. (The form of (3) changes slightly depending on the choice of permeability measure). The restriction to plane strain reduces the full set of equations to four equations in the three stresses σ_{xx}, σ_{yy}, σ_{xy} (positive in tension) and the excess pore pressure p. The assumption of steady motion at speed v is a further simplification; and the equations to be solved then are [13]:

$$\partial\sigma_{xx}/\partial x + \partial\sigma_{xy}/\partial y = 0 \;,\; \partial\sigma_{xy}/\partial x + \partial\sigma_{yy}/\partial y = 0 \qquad (4a)$$

$$\left[\frac{\partial^2}{\partial x^2} + \frac{\partial^2}{\partial y^2}\right]\left[\sigma_{xx} + \sigma_{yy} + \frac{3(\nu_u - \nu)}{(1+\nu_u)(1-\nu)} p\right] = 0 \qquad (4b)$$

$$\left[\frac{\partial^2}{\partial x^2} + \frac{\partial^2}{\partial y^2} + \frac{v}{c}\frac{\partial}{\partial x}\right]\left[\sigma_{xx} + \sigma_{yy} + \frac{3}{B(1+\nu_u)} p\right] = 0 \qquad (4c)$$

where $c = 2G\kappa B^2\beta(1+\nu_u)^2/(9(\nu_u - \nu))$ is the diffusivity and $\beta = (1-\nu)/(1-\nu_u)$. The drained ("slow") and undrained ("fast") Poisson's ratio are denoted by ν and ν_u, the elastic shear modulus by G, and B is the ratio of the induced pore pressure to the mean hydrostatic compressive stress under undrained conditions. The terms in brackets in (4c) are proportional to the fluid mass content

per unit volume. The coordinates x,y are fixed in the solid material.

Boundary Conditions

The coordinate axes are taken so that the advancing crack tip instantaneously coincides with the origin. Due to symmetry about the x-axis, the equations need only be solved for $y \geq 0$. The full boundary conditions are given by using: a) symmetry, b) the assumption that the crack faces are impermeable and so by eq. (3) $\partial p/\partial y$ is zero there, c) normal compressive loads $\tau(x)$ are applied to the crack faces, d) all stresses vanish very far from the crack tip. Together these give:

$$\begin{aligned} &\partial p(x,0)/\partial y = \sigma_{xy}(x,0) = 0 && \text{for } -\infty < x < \infty \\ &\partial \sigma_{xx}(x,0)/\partial y = 0 && \text{for } 0 < x < \infty \\ &\sigma_{yy}(x,0) = -\tau(x) && \text{for } -\infty < x < 0 \\ &p\ ,\ \sigma_{xx}\ ,\ \sigma_{yy}\ ,\ \sigma_{xy} \to 0 && \text{as } x^2 + y^2 \to \infty\ . \end{aligned} \tag{5}$$

SOLUTION

The equations (4) have only one characteristic length c/v. The physical problem, however, has two lengths: 1) the length ℓ over which loads are applied, and 2) the length ω of material breakdown. Three regimes of behavior are given by the relations of these lengths where it is always assumed that $\ell \gg \omega$.

Case I: $c/v \gg \ell \gg \omega$. In this case of very slow crack growth the excess pore pressure is totally drained in the general region of the crack face loading and response is exactly that of an elastic material with modulus G and Poisson's ratio ν and the excess pore pressure is zero everywhere. That is, $\sigma_{ij} = \sigma_{ij}^{\text{elastic}}$, $p \equiv 0$ and $K^{\text{elastic}} = K^{\text{porous elastic}}$. If this corresponds to crack growth then $K_{nom} = K_{crit}$ where K_{nom} is defined to be the stress intensity factor that the applied loads would cause on an ordinary elastic medium with drained properties.

Case II: $\ell \gg c/v \gg \omega$. In this intermediate range the material is undrained, or relatively stiffer, over the size scale of the applied loading and drained, or relatively softer over the region of material breakdown. The solution is here obtained by performing a fourier transform on equations (4) and solving the resulting ordinary differential equations [13] and then imposing the boundary conditions (5) and the Weiner-Hopf technique [15]. The loading $\tau^{\lambda}(x) \equiv e^{i\lambda x}$ for $x < 0$ (where $\text{Im}\{\lambda\} < 0$) results in an expression for $\sigma_{yy}(x,0)$ valid asymptotically as $x \to 0$. By superposing loads of the form $\tau^{\lambda}(x)$ the near tip stress field for the load $\tau(x) = \tau$ for $-\ell < x < 0$ ($\tau(x) = 0$ for $x < -\ell$) can be found. The results are that there is a stress singularity of the form (2) near the crack tip.

The applied load τ required to cause $K = K_{crit}$ would have caused a stress intensity factor $K_{nom} = \tau(\beta\pi\ell)^{\frac{1}{2}}$. The relation between K_{nom} and K_{crit} is then a measure of retardation effects. The expression is valid for all values of v and

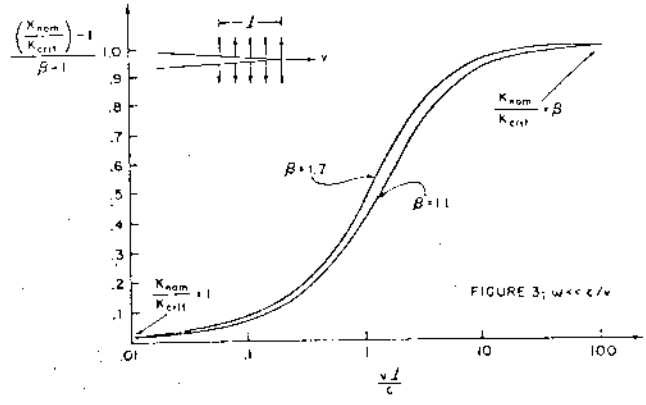

FIGURE 3; $\omega \ll c/v$

FIGURE 3; Stabilization when the criterion for crack growth is that the crack tip stress singularity is equal to a critical material value (i.e., $K=K_{crit}$,) the stress intensity factor the applied loads would have caused in an elastic material, K_{nom}, increases from K_{crit} to βK_{crit} as v increases from 0 to ∞.

results in

$$K_{nom} \to K_{crit} \quad \text{as} \quad v/(c/\ell) \to 0 \qquad (6a)$$

$$K_{nom} \to \frac{1-\nu}{1-\nu_u} K_{crit} = \beta K_{crit} \quad \text{as} \quad v/(c/\ell) \to \infty \qquad (6b)$$

Equations (6) say that the crack tip stress intensity is reduced by a factor β over what the loads would cause on an elastic material if v is large enough. The form of the relation between K_{nom} and K_{crit}, *vs.* v is given in figure 3 as evaluated numerically. The variables in the plot have been chosen to suppress the dependence of the form of the relation on β.

Case III: $\ell >> \omega >> c/v$. With this very fast crack growth material response is undrained everywhere but in a vanishing region around the crack tip and faces [15]. The results of equations (2), (6) and figure 3 are mathematically still valid but the range of validity is too small to be physically meaningful. The undrained elastic field causes a pore fluid suction which can be evaluated from the definition of B and the plane strain constraint. Using the effective stress criterion $\bar{\sigma}(\omega,0) = \bar{\sigma}_{crit}$, the following is obtained

$$K_{nom}/K_{crit} = (1-2B(1+\nu_u)/3)^{-1} \qquad (7)$$

where K_{crit} is now the stress intensity that the loads would have caused if material response were totally drained. The transition between the results of eq. (6b) where $\ell >> c/v >> \omega$ and eq. (7) where $\ell >> \omega >> c/v$ is given by [15]

$$\frac{K_{nom}}{K_{crit}} = \left\{1 - \frac{\nu_u-\nu}{1-\nu}\left[2e^{-\nu\omega/c} - \frac{c}{\nu\omega}(1-e^{-\nu\omega/c})\right] - 2B(1+\nu_u)(1-e^{-\nu\omega/c})/3\right\}^{-1} \qquad (8)$$

where (8) reduces to (6b) and (7) for small and large v respectively. The results of eq. (8) for a few values of the parameters ν, ν_u, B are plotted in figure 4. Equations (8) and (9) have been obtained using fourier transforms and are valid for any loading $\tau(x)$ which, if applied to an ordinary elastic material, would cause eq. (1) to be valid over a range large compared to both c/v and ω.

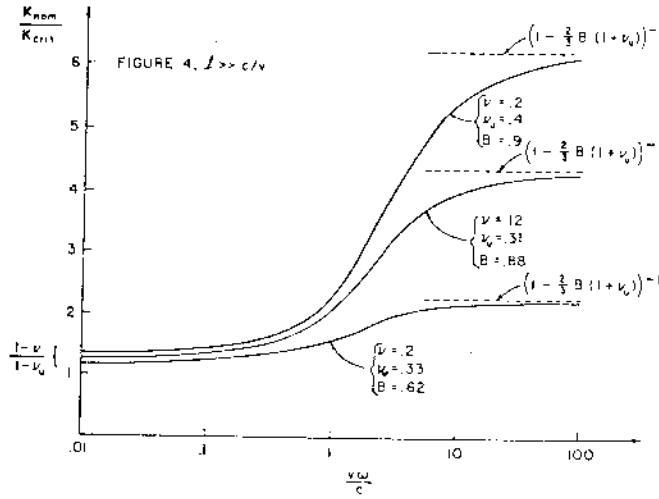

FIGURE 4; Stabilization when the crack growth criterion is that the effective tensile stress ahead of the crack tip reach a critical value, i.e., $\bar{\sigma}(\omega) = \bar{\sigma}_{crit}$. Applied loads may need to be much higher to cause fast growth than slow growth, depending on material properties.

The effect in equation (8) is due to pore fluid suction in the decohesion zone (or point), the full pore pressure field is given by

$$p(r,\theta) = \frac{-K_{nom}}{(2\pi r)^{\frac{1}{2}}} \frac{2B(1+\nu_u)}{3}(1-e^{-vr(1+\cos\theta)/2c})\cos(\theta/2) \qquad (9)$$

where θ is the angle from the x-axis. The level lines of the pore pressure are given in figure 5a and the values of the pore pressure on the x-axis in figure 5b. Note: the pore pressure is zero on the negative x-axis (crack faces) so the assumption of impenetrability of the crack faces is not necessary if $\ell >> c/v$.

DISCUSSION

Two mechanisms of retardation of hydraulic

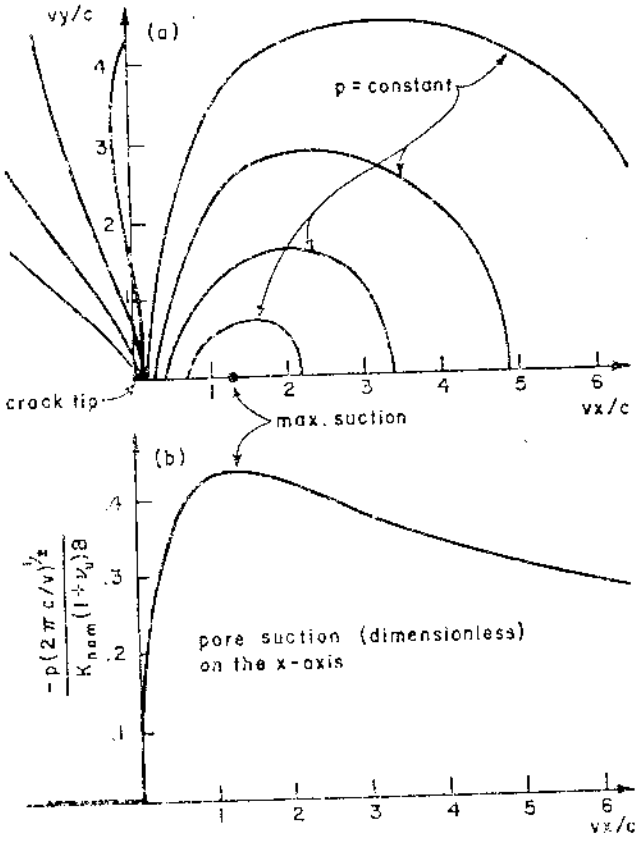

FIGURE 5; Pore pressure field near the crack tip for $t \gg c/v$. (a) Lines of constant pore pressure, (b) Dimensionless pore suction (-p) on the x-axis.

fracture have been examined mathematically. The first is due to the fact that material response turns out to be, in effect, inhomogeneous, with the material near the crack tip behaving in a softer (drained) manner than the far away (undrained) material. The effect can also be thought of as being due to energy dissipated in the flow of pore fluid. The second effect is due to the fact that a pore fluid suction (or at least a pressure less than ambient pressure) is induced in the region of material breakdown at the crack tip thus decreasing the effective tensile stresses in that region. The model used to investigate this second effect is very simple but any decohesion model is expected to yield similar results.

The magnitude of the mentioned effects and the speed of crack propagation at which they occur is extremely dependent on material properties. The Poisson ratios obey the constraint that $0 \leq \nu \leq \nu_u \leq .5$ and thus $1 \leq B \leq 2$. The diffusivity may vary in the range $10^{-5} m^2/sec < c < 10^{2} m^2/sec$ [12] and the pore pressure coefficient obeys the constraint $0 \leq B \leq 1$. For reasonable numerical estimations we can take $1.1 \leq \beta \leq 1.3$, $10^{-3} m^2/sec \leq c \leq 10^{-1} m^2/sec$, $.5 \leq B \leq .9$ [12].

From fig. 3 it is quickly seen that K_{nom} is required to increase to βK_{crit} at maximum. With $B \approx 1.2$ we see the first effect is fairly weak and probably easily dominated by inhomogeneities in the fracture toughness, K_{crit}, of the rock.

The second, effective stress, effect can be much stronger as illustrated in fig. 4. The load required to cause fracture may be several times the load required to fracture a drained specimen of the same rock (as is reflected in the values of K_{nom}/K_{crit}). This second effect becomes important as v becomes greater than about $4c/\omega$ (see fig. 4). The decohesion length, ω, can be estimated by comparing fracture toughness and tensile failure tests of the same drained rock type. Tests of an oil shale [17] for a particular orientation have given $K_{crit} \approx 1.1$ MPa-$m^{\frac{1}{2}}$ and tensile strength of about 15MPa thus implying $\omega \approx .85$ mm. If $c = 10^{-2} m^2/sec$ this gives a velocity of about $v \approx 50$ m/sec at which the effect becomes important.

The calculations here are based on a continuum model and we cannot expect, for example, that the pore fluid flow can be described so simply (Darcy's law) over the size scale of ω. Thus the results must be regarded as approximate.

The conclusions reached here may be expected to be applicable to cracks of any geometry where the crack tip conditions are approximately plane strain. Models of hydraulic fracture can most simply take account of these effects by modeling the rock as ordinary linear elastic with velocity dependent fracture toughness given by what is called K_{nom} in eq. 8.

Acknowledgements

This work has been funded by Brown University, The National Science Foundation and the U.S. Geological Survey. Discussions with James R. Rice and Donald A. Simons were essential for the completion of this work.

References:

[1] Abe, H., Mura, T. and Keer, L.M., Growth Rate of a Penny-Shaped Crack in Hydraulic Fracturing of Rocks, J.G.R., Vol. 81, No. 29 and No. 35, pgs. 5335-5340 and pgs. 6292-6298, Oct. and Dec., 1974.

[2] Cleary, M.P., PhD. Thesis, Brown Univ., Providence, R.I., December 1975.

[3] Cleary, M.P., Some Effects of Rate and Structure in Hydraulic Fracturing of Fluid-Saturated Porous Media, to be published in J. of Pet. Tech.

[4] Friedman, M., Porosity, Permeability, and Rock Mechanics - A Review, Proceedings; 17th Symposium on Rock Mechanics, 1976.

[5] Geertsma, J., Problems of Rock Mechanics in Petroleum Production Engineering, Proc. First Cong. Int. Soc. of Rock Mech., 1966.

[6] Geertsma, J. and deKlerk, F., A Rapid Method of Predicting Width and Extent of Hydraulically Induced Fractures, J. Pet. Tech., Dec. 1969.

[7] Haimson, B. and Fairhurst, C., Hydraulic Fracturing in Porous-Permeable Materials, SPE 2354, Soc. Pet. Eng.

[8] Howard, G.C. and Fast, C.R., Hydraulic Fracturing, Soc. Pet. Eng., Monograph Vol. 2, 1970.

[9] Jaeger, J.C. and Cook, N.G.W., Fundamentals of Rock Mechanics, Chapman and Hall, London, 1976.

[10] Mahmoud and Clifton, In progress.

[11] Nordgen, R.P., Propagation of a Vertical Hydraulic Fracture, Soc. Pet. Eng., Vol. 253, 1972.

[12] Rice, J.R. and Cleary, M.P., Some Basic Stress Diffusion Solutions for Fluid-Saturated Elastic Porous Media With Compressible Constituents, Rev. Geophys. Space Phys., 14, pgs. 227-241, May 1976.

[13] Rice, J.R. and Simons, D.A., The Stabilization of Spreading Shear Faults by Coupled Deformation-Diffusion Effects in Fluid-Infiltrated Porous

[14] Roegiers, J.C. and Brown, D.W., Geothermal Energy: A New Application of Rock Mechanics, Proc. 3rd Cong. Int. Soc. Rock Mech., Denver, II, A, 674, 1974.

[15] Ruina, A.L., Masters Thesis, Brown Univ., Providence, R.I., June 1978. Appendices.

[16] Seed, H.B., Leps, T.M., Duncan, J.M. and Bieber, R.S., Hydraulic Fracturing and its Possible Role in the Teton Dam Failure, in Report to U.S. Dept. of Int. and State of Idaho on Failure of Teton Dam by Independent Panel to Review Causes of Teton Dam Failure, Appendix D, Dec. 1976.

[17] Schmidt, R.A. and Huddle, C.W., Fracture Mech. of Oil Shale: Some Preliminary Results, Feb. 1977, Sandia Laboratories, internal publication.

[18] Simons, D.A., Boundary-Layer Analysis of Propagating Mode II Cracks in Porous Elastic Media, J. Mech. Phys. Solids, 1977.

[19] Tada, H., Paris, P.C. and Irwin, G.R., The Stress Analysis of Cracks, pub. by Del Res. Co., Hellertown, Pa. 1973.

[20] Terzaghi, K. and Peck, R.B., Soil Mechanics in Engineering Practice, John Wiley & Sons, N.Y., 1967.

APPENDIX I

Field Equations

A brief derivation of Rice and Cleary's [12] form of Biot's constitutive equations for small deformations of a fluid saturated, isotropic, linear-elastic porous solid follows. The derivation of the analogous equations for coupled deformation-diffusion of a solid (like steel) containing a mobile chemical species (like hydrogen) and linear coupled thermo-elasticity are exactly the same with suitable redefinition of terms.

The stress σ_{ij}, the strain ε_{ij}, the fluid mass content ζ and the pore pressure p may be regarded as excesses relative to a state σ^o_{ij}, ε^o_{ij}, p^o, m^o in which body forces are equilibrated — the constitutive equations must then be interpreted appropriately.

The strain of the solid phase is assumed to depend linearly and isotropically on the stress σ_{ij} and the pore pressure p, thus

$$2G\varepsilon_{ij} = \sigma_{ij} - (\nu/(1+\nu))\delta_{ij}\sigma_{kk} + C_1 p\delta_{ij} \quad , \tag{I.1}$$

where the form of (I.1) is found by looking separately at the cases where $\sigma_{ij} = 0$ or $p = 0$. The shear modulus is G and the <u>drained</u> Poisson ratio is ν. The pore pressure p is defined as the pressure in a container that contains pure pore fluid, or diffusing chemical, and is in equilibrium against matter transfer with the ambient pore fluid, or diffusing chemical — this value cannot necessarily be identified with any simple definition of fluid pressure inside the solid. In the case of thermo-elasticity, p should be replaced by the deviation in the temperature and ν is the isothermal Poisson ratio.

The alteration in fluid mass content per unit reference volume of solid is assumed to be linearly and isotropically dependent on the total stress σ_{ij} and the pore pressure p. This relation can be expressed in terms of the two independent constants C_2 and B as

$$\Delta m/\rho^{o} = (C_2/2G)\left[\sigma_{kk} + (3/B)p\right] \tag{I.2}$$

where ρ^{o} is the pore fluid density. The variable B is a material constant (Skempton's pore pressure coefficient) which can be interpreted from the result that $p = -B\sigma_{kk}/3$ in an experiment that measures induced pore pressure for stressing under totally undrained conditions ($\Delta m = 0$). In thermo-elasticity $\Delta m/\rho^{o}$ should be replaced with alteration in entropy content.

From the assumed existence of an energy density, the free energy ϕ can be shown to satisfy the following differential relation (thermal effects neglected):

$$d\phi(\varepsilon_{ij},m) = \sigma_{ij}d\varepsilon_{ij} + \left[\int_{p^{o}}^{p} \frac{dp'}{\rho(p')}\right]dm \ . \tag{I.3}$$

The two Legendre transforms on Eq. (I.3) give

$$d[\text{something}] = \varepsilon_{ij}d\sigma_{ij} + (m/\rho(p))dp \ , \tag{I.4}$$

from which follow the reciprocal relations

$$(\partial\varepsilon_{ij}/\partial p)_{\sigma_{\text{fixed}}} = (\partial(m/\rho)/\partial\sigma_{ij})_{p_{\text{fixed}}} \ , \tag{I.5}$$

which imply that the constants C_1 and C_2 in (I.1) and (I.2) are equal to each other. In thermo-elasticity "[something]" is the Gibbs free energy and other terms should be identified as before.

The material must behave as an ordinary elastic material under totally undrained conditions(since p is no longer then an independent variable) with the same shear modulus G as under drained conditions (since shear is unaffected by pore pressure variations in (I.1)), but with a different Poisson ratio, denoted by ν_u. In thermo-elasticity, ν_u is the isentropic Poisson ratio. Equation (I.1) must then reduce to $2G\epsilon_{ij} = \sigma_{ij} - (\nu_u/(1+\nu_u))\delta_{ij}\sigma_{kk}$ under undrained conditions $(\Delta m = 0)$. Equating this relation with (I.1) expressed in terms of ν and $p = -B\sigma_{kk}/3$ yields $C_1 = C_2 = 3(\nu_u-\nu)/(B(1+\nu)(1+\nu_u))$.

The third constitutive law is that of Darcy which relates the ambient pore fluid flow linearly and isotropically to the excess pore pressure (the excess in pore pressure over the pressure field that equilibrates all body forces - assumed to be derived from a potential) gradient,

$$q_i = -\rho^o \kappa \partial p/\partial x_i \ ; \qquad (I.6)$$

where q_i is the mass flux rate of pore fluid across a surface of unit area fixed in the material with normal in the i-direction. The permeability is given by κ. In linear thermo-elasticity q_i/ρ^o should be replaced by the heat flux vector divided by absolute reference temperature (entropy flux), Equation (I.6) is then a statement of Fourier's law of heat conduction. The remaining field equations are those of equilibrium, compatability and conservation of fluid mass content. In two dimensions, with inertial terms

neglected, equilibrium is expressed by

$$\partial\sigma_{xx}/\partial x + \partial\sigma_{xy}/\partial_y = 0 \quad , \quad \partial\sigma_{xy}/\partial x + \partial\sigma_{yy}/\partial_y = 0 \quad . \tag{I.7}$$

In plane strain, compatability (the condition necessary for the existence of a unique displacement field) is expressed by

$$\partial^2\varepsilon_{xx}/\partial y^2 + \partial^2\varepsilon_{yy}/\partial x^2 = 2\partial^2\varepsilon_{xy}/\partial x\partial y \quad . \tag{I.8}$$

When the constitutive law I1 is modified by the plane strain constraint that $\varepsilon_{zz} = 0$ and applied to compatability (I.8), and the result is simplified by use of equilibrium (I.7), we have the plane strain compatability equation expressed in terms of stresses and excess pore pressure: [12]:

$$\left(\frac{\partial^2}{dx^2} + \frac{\partial^2}{dy^2}\right)\left[\sigma_{xx} + \sigma_{yy} + \frac{3p}{B}\frac{(\nu_u-\nu)}{(1+\nu_u)(1-\nu)}\right] = 0 \quad . \tag{I.9}$$

The equation of fluid mass conservation is

$$\partial m/\partial t + \partial q_i/\partial x_i = 0 \quad . \tag{I.10}$$

In the thermo-elastic case with m/ρ_o replaced by entropy content and q_i/ρ_o with entropy flux (I.10) is a continuum statement of the combined 1st and 2nd laws of thermodynamics, where it is assumed that the actual stress is equal to the associated equilibrium stress.

The expression for changes in fluid mass content (I.2) can be modified for plane strain by means of (I.1) and then substituted into the 1st term in (I.10). Darcy's law (I.6) can be substituted into the second term in (I.10) to obtain an expression for the conservation of fluid mass in

terms of stress and pore pressure gradient. This result, multiplied by an appropriate factor, can be added to the compatability relation (I.9) to give the following diffusion equation [12]:

$$\left[\frac{\partial^2}{\partial x^2} + \frac{\partial^2}{\partial y^2} - \frac{1}{c}\frac{\partial}{\partial t}\right]\left[\sigma_{xx} + \sigma_{yy} + \frac{3}{B(1+\nu_u)}p\right] = 0 \qquad \text{(I.11)}$$

where

$$c = \kappa\left[\frac{2G(1-\nu)}{(1-2\nu)}\right]\left[\frac{B^2(1+\nu_u)^2(1-2\nu)}{9(1-\nu_u)(\nu_u-\nu)}\right]$$

is the diffusivity and where $[\sigma_{xx} + \sigma_{yy} + 3p/(B(1+\nu_u))]$ is proportional to the alteration in fluid mass content, Δm .

In our problem, we are assuming the steady state condition that all distributions of field variables move at speed v with the crack tip. Expressed mathematically, this is $f(x,y,t) = f(x-vt,y)$, which implies that $\frac{\partial f}{\partial t} = -v\frac{\partial f}{\partial x}$ for any field variable f . This result can be applied to the diffusion equation (I.11) to give [13]:

$$\left[\frac{\partial^2}{\partial x^2} + \frac{\partial^2}{\partial y^2} + \frac{v}{c}\frac{\partial}{\partial x}\right]\left[\sigma_{xx} + \sigma_{yy} + \frac{3}{B(1+\nu_u)}p\right] = 0 \ . \qquad \text{(I.12)}$$

Equations (I.7),(I.9) and (I.12) now constitute a set of four equations in the four stress variables σ_{xx} , σ_{yy} , σ_{xy} and p .

APPENDIX II

Boundary Conditions

The coordinate axes are taken so that the origin instantaneously coincides with the crack tip and the x-axis is parallel with the direction of crack growth. Due to symmetry about the x-axis, the equations only need to be solved for $y \geq 0$ with appropriate boundary conditions.

On physical grounds it can be seen that three boundary conditions are required on all boundaries; for example, two components of traction and the pore pressure. In our case the boundary conditions are supplied by the following assumptions and observations:

a) There is no fluid flow across the crack faces and thus by Darcy's law (I.6), $\partial p/\partial y$ is zero there. The pore pressure field is differentable and symmetric so $\partial p/\partial y$ is zero on the x-axis ahead of the crack tip also.

b) No shear loads are applied to the crack faces so $\sigma_{xy} = 0$ there. Symmetry implies that $\sigma_{xy} = 0$ also on the x-axis ahead of the crack tip.

c) $\sigma_{yy} = -\tau$ on the crack faces.

d) Differentiability and symmetry imply that $\partial\sigma_{xx}/\partial y = 0$ on the x-axis ahead of the crack tip.

e) All field variables must go to zero with increasing distance from the crack tip. Together, these are:

$$\partial p(x,0)/\partial y = 0 \quad \text{for} \quad -\infty < x < \infty \tag{II.1}$$

$$\sigma_{xy}(x,0) = 0 \quad \text{for} \quad -\infty < x < \infty \tag{II.2}$$

$$\sigma_{yy}(x,0) = -\tau(x) \quad \text{for} \quad -\infty < x < 0 \tag{II.3}$$

$$\partial\sigma_{xx}(x,0)/\partial y \quad \text{for} \quad 0 < x < \infty \tag{II.4}$$

$$p \, , \, \sigma_{xx} \, , \, \sigma_{yy} \, , \, \sigma_{xy} \to 0 \quad \text{as} \quad x^2+y^2 \to \infty \tag{II.5}$$

Condition (II.4) can be expressed as

$$\frac{\partial}{\partial y}\int_{o}^{x}\sigma_{xx}(x,y)dx\Big|_{y=0} = 0 \quad \text{for} \quad 0 < x < \infty \tag{II.6}$$

for future calculations.

APPENDIX III

Limiting Cases

Some results can be inferred for certain limiting cases without recourse to fourier transforms and the Weiner-Hopf technique. These cases have been noticed in [3] for Mode I cracks and some of them are discussed at length in [18] for the analogous Mode II (shear) problem.

The only characteristic length in the governing equations (I.7), (I.9) and (I.12) is c/v , the ratio of the diffusivity to the crack propagation velocity. There are two other lengths however, in the physical problem being analyzed. One is ℓ , the length over which the crack face load is applied; the other is ω , the size of the breakdown zone. Throughout our discussion, we assume $\ell >> \omega$.

Different regimes of behavior are determined by the relative size of c/v , ℓ and ω .

Case I: $c/v >> \ell >> \omega$. In this case of very slow crack growth, all excess pore pressure is totally drained in the general region of the crack face loading and the response is that of an elastic material with drained properties. This result is intuitively acceptable, but can be justified by substituting $\hat{x} = x/\ell$, $\hat{y} = y/\ell$ into the equations (I.7), (I.9) and (I.12) and noting the limiting form of these equations as c/v gets much larger than ℓ . There result the equations

$$\frac{\partial \sigma_{xx}}{\partial \hat{x}} + \frac{\partial \sigma_{xy}}{\partial \hat{y}} = 0 \qquad \left(\frac{\partial^2}{\partial \hat{x}^2} + \frac{\partial^2}{\partial \hat{y}^2}\right)\left(\sigma_{xx} + \sigma_{yy}\right) = 0$$

$$\frac{\partial \sigma_{xy}}{\partial \hat{x}} + \frac{\partial \sigma_{yy}}{\partial \hat{y}} = 0 \qquad \left(\frac{\partial^2}{\partial \hat{x}^2} + \frac{\partial^2}{\partial \hat{y}^2}\right) p = 0 \quad . \tag{III.1}$$

For the boundary conditions given, (II.1) - (II.6), these equations have the unique solution $p \equiv 0$ and $\sigma_{ij} = \sigma_{ij}^{elastic}$ where the character of the equations in the far field is assumed to have no influence. That is, the stress field is exactly that which the same loads would cause on an ordinary elastic material. In particular, the stress intensity factor observed at the crack tip is exactly the same as would be predicted for an elastic material. This can be expressed by saying that at very low speeds, fracture propagation requires $K_{nom} = K_{crit}$ where K_{nom} is defined as the stress intensity that the applied loads would cause on an elastic medium, and K_{crit} is a material property. In this limiting case, nothing is gained by looking at effective stresses or a breakdown zone.

Case II: $\ell >> c/v >> \omega$. In this intermediate range, the material is undrained ($\Delta m=0$) , or relatively stiffer over the size scale of the applied loading (or crack length) and drained, or relatively softer, over the region of material breakdown. This case cannot be discussed carefully without more detailed calculation. A physical argument based on matching near tip and far from tip displacement fields is presented in [13] to justify the results to be shown. The transition between the results for this case and cases I and III will also be shown.

Case III: $\ell >> \omega >> c/v$. In this very high speed limit, the material behavior (away from a vanishing range near the crack tip and faces) is totally undrained. That is, crack growth is sufficiently fast that there is no time for diffusion of pore fluid (except possibly at the immediate crack tip and crack faces). This can be demonstrated by the same substitution as before ($\hat{x} = x/\ell$, $\hat{y} = y/\ell$) . Now equations (I.7), (I.9) and (I.12)

become (with $\ell/(c/v) \to \infty$) [18]:

$$\frac{\partial \sigma_{xx}}{\partial \hat{x}} + \frac{\partial \sigma_{xy}}{\partial \hat{y}} = 0 \qquad \text{(III.2)}$$

$$\frac{\partial \sigma_{xy}}{\partial \hat{x}} + \frac{\partial \sigma_{yy}}{\partial \hat{y}} = 0 \qquad \text{(III.3)}$$

$$\left(\frac{\partial^2}{\partial \hat{x}^2} + \frac{\partial^2}{\partial \hat{y}^2}\right)\left[\sigma_{xx} + \sigma_{yy} + 2\eta p\right] = 0 \qquad \text{(III.4)}$$

$$\frac{\partial}{\partial \hat{x}}\left[\sigma_{xx} + \sigma_{yy} + \frac{3}{B(1+\nu_u)}\, p\right] = 0 \qquad \text{(III.5)}$$

where $\eta = 3(\nu_u-\nu)/[2B(1+\nu_u)(1-\nu)]$ and the bracketed term in (III.5) is proportional to the alteration of fluid mass content.

The boundary conditions imply that the bracketed term in (III.5) vanish as $\hat{x} \to \infty$ so, by inspection it must vanish everywhere. Thus, the material response is undrained. This gives the result that $p = -(1+\nu_u)B(\sigma_{xx} + \sigma_{yy})/3$ everywhere (that is, everywhere where $\hat{x} = 1$). Applied to (III.4), we again have the standard equations of linear elasticity. A result of the solution of these equations for our geometry is [19] $\sigma_{yy}(\hat{x},0) = K(2\pi\hat{x})^{-1/2} = \sigma_{xx}(\hat{x},0)$ for $\hat{x}$ small. From this and the undrained condition, the pore pressure $p(\hat{x},0)$ on the x-axis can be found as can $\bar{\sigma}(\hat{x},0) \equiv \sigma(\hat{x},0) + p(\hat{x},0)$. We have then that

$$\bar{\sigma}_{yy}(\hat{\omega},0) = \left[1 - 2B(1+\nu_u)/3\right] K_{nom}/(2\pi\omega)^{1/2} \quad . \qquad \text{(III.6)}$$

In carrying out this limit the region in which $x^2 + y^2 \lesssim c^2/v^2$ was shrunk to a point at the crack tip. Thus, the field found for the arguments

$\hat{x},\hat{y}$ carries, in this case, no information about the values of the field variables inside the region with radius of order c/v .

APPENDIX IV

Fourier Transform and Weiner Hopf Technique

The full analysis of the problem is carried out by use of fourier transforms. In particular, any field variable, f, is related to its transform $\tilde{f}$ by:

$$\tilde{f}(\kappa,y) = \int_{-\infty}^{\infty} f(x,y)e^{-i\kappa x}dx \qquad \text{(IV.1a)}$$

$$f(x,y) = \frac{1}{2\pi}\int_{-\infty}^{\infty} \tilde{f}(\kappa,y)e^{i\kappa x}d\kappa \quad , \qquad \text{(IV.1b)}$$

where $i = \sqrt{-1}$ and κ is a new variable used in the transform (not to be confused with permeability). The transform can be applied to (I.7), (I.9) and (I.12) to give

$$i\kappa\,\tilde{\sigma}_{xx}(\kappa,y) + \frac{\partial}{\partial y}\tilde{\sigma}_{xy}(\kappa,y) = 0 \qquad \text{(IV.2a)}$$

$$\frac{\partial}{\partial y}\tilde{\sigma}_{xy}(\kappa,y) + i\kappa\,\tilde{\sigma}_{xy}(\kappa,y) = 0 \qquad \text{(IV.2b)}$$

$$\left[-\kappa^2 + \frac{\partial^2}{\partial y^2}\right]\left[\tilde{\sigma}_{xx}(\kappa,y) + \tilde{\sigma}_{yy}(\kappa,y) + \frac{3p}{B}\frac{(\nu_u-\nu)}{(1+\nu_u)(1-\nu)}\right] = 0 \qquad \text{(IV.2c)}$$

$$\left[i\kappa v/c = \kappa^2 + \partial^2/\partial y^2\right]\left[\tilde{\sigma}_{xx}(\kappa,y) + \tilde{\sigma}_{yy}(\kappa,y) + (3/(B(1+\nu)))\,\tilde{p}(\kappa,y)\right] = 0 \,. \qquad \text{(IV.2d)}$$

These are four ordinary differential equations in four variables. They can be solved in terms of the yet to be determined constants (constant with respect to y) $a = a(\kappa)$, $b = b(\kappa)$, $d = d(\kappa)$, (see [3], [13]);

$$\tilde{\sigma}_{xx} = -[d + (my-1)a]e^{-my} + [1 - (\kappa^2+n^2)/(\kappa^2-n^2)]be^{-ny} \qquad \text{(IV.3a)}$$

$$\tilde{\sigma}_{yy} = [d + (my+1)a]e^{-my} + [1+(\kappa^2+n^2)/(\kappa^2-n^2)]be^{-ny} \qquad \text{(IV.3b)}$$

$$\tilde{\sigma}_{xy} = -[i\kappa d/m + i\kappa ya]e^{-my} - [2i\kappa n/(\kappa^2-n^2)]be^{-ny} \qquad \text{(IV.3c)}$$

$$\tilde{p} = \frac{2B(1+\nu_u)(1-\nu)}{3(\nu_u-\nu)}\left[-\frac{\nu_u-\nu}{1-\nu}\, ae^{-my} - be^{-ny}\right] \qquad \text{(IV.3d)}$$

where, in order to eliminate solutions that grow exponentially with y, $m = m(\kappa)$ and $n = n(\kappa)$ are defined such that:

$$m^2(\kappa) = \kappa^2 \quad , \quad \mathrm{Re}\{m(\kappa)\} \geq 0$$

$$n^2(\kappa) = \kappa^2 - i\kappa v/c \quad , \quad \mathrm{Re}\{n(\kappa)\} \geq 0 \quad . \qquad \text{(IV.4)}$$

Any analytic functions $a(\kappa)$, $b(\kappa)$ and $d(\kappa)$ that lead to well defined inverse transformations will result in solutions to the field equations.

The boundary conditions (II.1) - (II.6), can also be transformed by (IV.1a) and the results expressed in terms of a, b, and d from (IV.3):

$$m\mu a + nb = 0 \qquad \text{(IV.5a)}$$

$$2nb/(\kappa^2-n^2) + d/m = 0 \qquad \text{(IV.5b)}$$

$$a + [1 + (\kappa^2+n^2)/(\kappa^2-n^2)]b + d = -\tilde{\tau}(\kappa) + F^-(\kappa) \qquad \text{(IV.5c)}$$

$$-2ma + 2n^3/(\kappa^2-n^2) + md = G^+(\kappa) \qquad \text{(IV.5d)}$$

where

$$F^-(\kappa) \equiv \int_0^\infty \sigma_{yy}(x,0)e^{-i\kappa x}dx$$

$$G^+(\kappa) \equiv i\kappa\int_{-\infty}^0 e^{-i\kappa x}\frac{\partial}{\partial y}\int_0^x \sigma_{xx}(x',y)dx'dx$$

$$\mu \equiv (\nu_u-\nu)/(1-\nu) \quad .$$

Though the transform inversions are carried out for κ as a real variable we make use of the fact that the equations make sense for κ a complex variable. First, notice is made (for later use) that the unknown functions F^- and G^+ are analytic functions in the lower and upper κ plane respectively. Equations (IV.5a), (IV.5b) and (IV.5d) can be solved simultaneously for a, b and d in terms of G^+. This gives

$$a(\kappa) = \frac{G^+(\kappa)}{2m(\kappa)(\mu-1)} ,$$

$$b(\kappa) = \frac{-\mu\, G^+(\kappa)}{2n(\kappa)(\mu-1)} , \qquad \text{(IV.6)}$$

$$d(\kappa) = \frac{m(\kappa)\mu\, G^+(\kappa)}{(\mu-1)(\kappa^2-n^2)} .$$

This result can be applied directly to (IV.5c) to give, after some manipulation,

$$\frac{G^+(\kappa)}{2(\mu-1)m(\kappa)}\left[1 + \frac{2i\mu c}{v}\,\kappa\left(\frac{m(\kappa)}{n(\kappa)} - 1\right)\right] = F^-(\kappa) - \tilde{\tau}(\kappa) . \qquad \text{(IV.7)}$$

This is apparently a single equation in the two unknowns $F^-(\kappa)$ and $G^+(\kappa)$. However, it can be solved by the following device which is the substance of the Weiner-Hopf technique. The idea is to rewrite (IV.7) in such a way that the two sides are analytic functions in two overlapping half planes of the complex plane. This is done by factorizing the functions $m(\kappa)$ and $n(\kappa)$ (see (IV.4), as follows:

$$m(\kappa) = m^+(\kappa)m^-(\kappa) , \quad n(\kappa) = m^+(\kappa)n^-(\kappa) , \qquad \text{(IV.8)}$$

where $m^+(\kappa) = \kappa^{1/2}$ with branch cut on the negative imaginary axis,

$m^-(\kappa) = (\kappa - i\varepsilon)^{1/2}$ with branch cut on the positive imaginary axis from $i\varepsilon$ to $i\infty$ and with $\varepsilon > 0$ an arbitrarily small constant, later to be made to approach zero, and $n^-(\kappa) = (\kappa - iv/c)^{1/2}$ with branch cut on the positive imaginary axis from iv/c. The superscripts $+$ and $-$ refer to the upper and lower half planes (respectively) over which the functions are analytic. By using the decomposition (IV.8), equation (IV.7) is immediately separated as desired (closely parallel to [13])

$$\frac{G^+(\kappa)}{2(\mu-1)m^+(\kappa)} = \frac{[F^-(\kappa) - \tilde{\tau}(\kappa)]m^-(\kappa)}{D^-(\kappa)} \quad , \qquad \text{(IV.9)}$$

where

$$D^-(\kappa) = 1 + \frac{2i\mu c\kappa}{v}\left[\frac{m^-(\kappa)}{n^-(\kappa)} - 1\right] \quad .$$

For $\mathrm{Im}(\kappa) \leq 0$ and $v > 0$, we have $n^-(\kappa) \neq 0$, and so $D^-(\kappa)$ is analytic for all $\mathrm{Im}(\kappa) \leq 0$. It has the limiting values $D^-(0) = 1$ and $D^-(\kappa) \to 1-\mu = (1-\nu_u)/(1-\nu)$ as $|\kappa| \to \infty$. The function $D^-(\kappa)$ also has no zeros in the lower half κ plane.

Transition from Case I to Case II

Three different loadings, $\tau(x)$, will be used in the solution. The first two will give the principal result for limiting case II as well as the transition from case I to case II. First $\tau(x)$ will be taken as constant over a length ℓ representing the fracture length; $\tau(x) = \tau$ for $-\ell \leq x \leq 0$. Instead of using $\tau(x)$ directly in the solution, it is to be thought of as a superposition of loads of the form $\tau^\lambda(x) = e^{i\lambda x}$ for $x < 0$ where λ has a small negative imaginary part (i.e., $\tau^\lambda(-\infty) = 0$). The crack face loading can be reconstructed by the superposition integral

$$\tau(x) = \frac{1}{2\pi}\int_{-\infty}^{\infty}\tilde{\tau}(\lambda)\tau^{\lambda}(x)d\lambda = \frac{1}{2\pi}\int_{-\infty}^{\infty}\tilde{\tau}(\lambda)e^{i\lambda x}d\lambda \qquad \text{(IV.10)}$$

where $\tilde{\tau}(\lambda)$ is the density of $\tau^{\lambda}(x)$ in $\tau(x)$, and is found from

$$\tilde{\tau}(\lambda) = -(\tau/i\lambda)(1-\exp(i\lambda\ell)) \quad . \qquad \text{(IV.11)}$$

By the same superposition the value of any field quantity can be found from the value of that quantity due to the load $\tau^{\lambda}(x)$.

$$f = \frac{1}{2\pi}\int_{-\infty}^{\infty} f^{\lambda}\tilde{\tau}(\lambda)d\lambda \quad , \qquad \text{(IV.12)}$$

where f^{λ} is the response to $\tau^{\lambda}(x)$.

For our initial calculation we use $\tau^{\lambda}(x)$ as the loading. From (I.8a) its transform is found to be

$$\tilde{\tau}^{\lambda}(\kappa) = 1/[i(\lambda-\kappa)] \quad . \qquad \text{(IV.13)}$$

This is now applied to (IV.9), to which the same term is added to both sides of the equation to obtain

$$\frac{G^{+}(\kappa)}{m^{+}(\kappa)} + \frac{m^{-}(\lambda)}{D^{-}(\lambda)i(\lambda-\kappa)} = \frac{1}{i(\lambda-\kappa)}\left[\frac{m^{-}(\lambda)}{D^{-}(\lambda)} - \frac{m^{-}(\kappa)}{D^{-}(\kappa)}\right] + \frac{m^{-}(\kappa)}{D^{-}(\kappa)}F^{-}(\kappa) \quad . \qquad \text{(IV.14)}$$

This equation (similar to A15 in [13]), though originating from use with real values of κ, has been separated so that the left and right sides are analytic in all of the upper and lower complex κ plane respectively. For κ real, the two sides of (IV.14) are identical. Each can be analytically continued in a unique way to all of either the upper or lower

κ plane, and thus both sides of the equation are representations of a function that is analytic in the whole κ plane (entire function).

Examination of the right-hand side of Eq. (IV.14) shows that the entire function is bounded by a constant as $|\kappa| \to \infty$ with $\mathrm{Im}\{\kappa\} < 0$ and thus the function is a constant. This can be seen since the first term on the right side of (IV.14) is of order $\kappa^{1/2}F^-(\kappa)$ as $\kappa \to \infty$. However, by looking at the arguments used in limit case I and replacing ℓ by x^*, a typical point inside the "drained region," $x^* << c/v$, it is seen that the material response is of the ordinary linear elastic type in this range (even though we cannot yet say $p=0$ in this case) and thus by standard results of linear elastic fracture mechanics the stress field must have the form of Eq. (2) (i.e., σ_{ij} is of order $x^{-1/2}$ as $x \to 0$) where the K will depend on the far field in a way about to be shown. When this is applied to the definition of $F^-(\kappa)$, (IV.5), the result is that $F^-(\kappa)$ is of the order $\kappa^{-1/2}$ as $\kappa \to \infty$ so the product $m^-(\kappa)F^-(\kappa)$ is finite as $\kappa \to \infty$.

Because the right side of (IV.14) is constant, it may be evaluated for any convenient value of κ. It is possible to do this evaluation for the case $\kappa \to 0$. Since $D^-(0)$ is finite, all terms are easily evaluated except the rightmost term. This is evaluated as follows:

Very far from the crack tip, the stress field must be of order less than r^{-1} for finite strain energy. When this requirement is applied to the definition of $F^-(\kappa)$ in (IV.5), it shows that $F^-(\kappa)$ is of order less than κ^{-2} as $\kappa \to 0$. This gives the result that

$$\frac{G^+(\kappa)}{m^+(\kappa)} + \frac{m^-(\lambda)}{D^-(\lambda)i(\lambda-\kappa)} = \frac{1}{i(\lambda-\kappa)}\left[\frac{m^-(\lambda)}{D^-(\lambda)} - \frac{m^-(\kappa)}{D^-(\kappa)}\right] + \frac{m^-(\kappa)}{D^-(\kappa)} F^-(\kappa)$$

$$= \frac{1}{i\lambda} \frac{m^-(\lambda)}{D^-(\lambda)} . \qquad \text{(IV.15)}$$

The stress intensity factor, K^λ, for the loading $\tau^\lambda(x)$ can be found by noting from (II.3) and (IV.5c) that

$$\tilde{\sigma}^\lambda_{yy}(\kappa,0) = 1/[i(\lambda-\kappa)] + F^-(\kappa) \qquad \text{(IV.16)}$$

where $F^-(\kappa)$ is found from the right side of Eq. (IV.15). It can be seen from (IV.15) and (IV.16) that $\tilde{\sigma}^\lambda_{yy}(\kappa,0)$ asymptotically approaches $[D^-(\infty)m^-(\lambda)/(i\lambda D^-(\lambda))]\kappa^{-1/2}$ as $\kappa \to \infty$. We already know that $\sigma_{yy}(x,0)$ has the form $K/\sqrt{2\pi x}$ as $x \to 0$, which implies that $\sigma_{yy}(x,0)$ has a Fourier transform which is asymptotically equal to $K(1-i)\kappa^{-1/2}/2$ as $\kappa \to \infty$. Comparing this to the result in the previous sentence, and using $D^-(\infty) \equiv 1/\beta = \frac{1-\nu_u}{1-\nu}$, we have

$$\beta K^\lambda = \frac{2}{i(1-i)} \frac{m^-(\lambda)}{\lambda D^-(\lambda)} . \qquad \text{(IV.16)}$$

To find the asymptotic stress intensity factor for the loading pictured in Figure 2b, we use the superposition outlined by equations (IV.11) and (IV.12):

$$\beta K = \frac{\tau}{(1-i)\pi} \int_{-\infty}^{\infty} \frac{m^-(\lambda)}{\lambda^2 D^-(\lambda)} [1 - \exp(i\lambda\ell)]d\lambda . \qquad \text{(IV.17)}$$

In this equation, $D^-(\lambda)$ also depends on ν, and material properties as seen in (IV.9). Equation (IV.17) can be re-expressed so that it is clear

that the dependence is only on the two dimensionless parameters $\beta = (1-\nu)/(1-\nu_u)$, $\gamma = v\ell/c$ and the loading as represented by the loading parameter $K_{nom} = \sqrt{8\pi\ell}$, [19], the stress intensity factor the same loads would cause on an elastic solid:

$$K = \frac{(1+i)K_{nom}}{4\sqrt{2\pi}} \int_{-\infty}^{\infty} \frac{s^{-3/2}(1-e^{is})}{\beta \hat{D}^{-}(s,\gamma)}\, ds \qquad \text{(IV.18)}$$

where

$$\hat{D}^{-}(s,\gamma) = 1 + \frac{2i(\beta-1)s}{\gamma\beta}\left[\frac{s^{1/2}}{(s-i\gamma)^{1/2}} - 1\right] = D^{-} \quad ,$$

and where all multivalued functions have branch cuts on the positive imaginary axis. The limiting values of $\hat{D}^{-}$ are

$$\hat{D}^{-}(s,\gamma) \to 1/\beta \quad \text{as} \quad \gamma \to 0 \; ; \; \hat{D}^{-}(s,\gamma) \to 1 \quad \text{as} \quad \gamma \to \infty \; . \qquad \text{(IV.19)}$$

The integral in (IV.18) is evaluated by changing the contour (as in [ ]) to one that wraps around the positive imaginary axis and calling $s = i\psi$. There results

$$K = \frac{K_{nom}}{2\beta\pi^{1/2}} \int_{0}^{\infty} \psi^{-3/2}(1-e^{-\psi}) \mathrm{Re}\left\{\frac{1}{\hat{D}(\psi/\gamma)}\right\} d\psi \qquad \text{(IV.20)}$$

where

$$\hat{D}(\psi/\gamma) = 1 - \frac{2(\psi/\gamma)(\beta-1)}{\beta}\left[(1-i)/(\psi/\gamma))^{-1/2} - 1\right] \quad .$$

Using the limiting values of $\hat{D}$ (same as limiting values of $\hat{D}^-$ in (IV.19)), and the fact that

$$\int_0^\infty \psi^{-3/2}(1-e^{-\psi})d\psi = 2\pi^{1/2} \quad ,$$

we obtain from (IV.20) that

$$K_{nom} \to K \quad \text{as} \quad \gamma = v\ell/c \to 0 \tag{IV.21a}$$

$$K_{nom} \to \beta K \quad \text{as} \quad \gamma = \frac{v\ell}{c} \to \infty \, . \tag{IV.21b}$$

Equations (IV.21) give, respectively, the results of limit case I and limit case II. These limiting values agree exactly with the results of [13] for the shear fault and agree qualitatively with the numerical results of [3]. The transition of (IV.21) from limit case I to limit case II is evaluated on the computer and shown in Figure 3. The results are essentially similar to those in Rice and Simons [13] Fig. 4 (where $G_{nom}/G_{crit} = K^2_{nom}/K^2_{crit}$) but, the transition from the slow limit value to the fast occurs in our case at about $v\ell/c = 1.5$ whereas for the shear crack, the transition occurs at about $v\ell/c = 10$. The result here is similar to those of Cleary [3] for an almost identical problem. His calculation however, is done using a loading that diminishes linearly from a value τ at the crack tip to zero a distance ℓ from the crack tip. Since the loading is weighted towards the crack tip, his loaded length is effectively less than ours; a greater value of ℓ should be required by him to obtain the same dimensionless increase in K_{nom} . That is, we would expect his curve to fall to the right of ours in Fig. 3. The fact that this does not happen may be partially explained by the material

response to a point load moving with the crack tip a distance ℓ behind.

Solution to Point Force

Take $\tau(x) = \tau\delta(x+\ell)$ where $\delta(x)$ is the Kronecker delta function. Use the transform (IV.1a) to get $\tilde{\tau}(\lambda) = e^{i\lambda\ell}$. Using the solution for K^{λ} of Eq. (VI.16) and the superposition of Eq. (IV.12), the result for K is found:

$$K = \frac{\tau}{\beta i(1-i)\pi\sqrt{\ell}} \int_{-\infty}^{\infty} S^{-1/2} e^{iS} / \hat{D}^{-}(S,\gamma)dS \quad . \tag{IV.22}$$

Using the result from Tada et al. [19] that this point load would cause the stress intensity factor $K_{nom} = \tau\sqrt{2/\pi\ell}$ and changing variables by $S = i\psi$ one obtains:

$$K = \frac{K_{nom}}{\beta\sqrt{\pi}} \int_{0}^{\infty} \psi^{-1/2} e^{-\psi} \mathrm{Re}\left\{\frac{1}{\hat{D}(\psi/\gamma)}\right\} d\psi \quad . \tag{IV.23}$$

Using the limiting values of $\hat{D}$ and the fact that

$$\int_{0}^{\infty} \psi^{-1/2} e^{-\psi} d\psi = \sqrt{\pi} \quad ,$$

we again obtain

$$\begin{aligned} K_{nom} &\to K \quad \text{as} \quad v\ell/c \to 0 \\ K_{nom} &\to \beta K \quad \text{as} \quad v\ell/c \to \infty \quad . \end{aligned} \tag{IV.24}$$

The details of the transition are found by evaluation of the integral (IV.23) on the computer, which is carried out for a range of values of β. It is noted that for this loading the peak stabilizing effect (considering the end zone to be infinitesimal) occurs at about $v\ell/c = 2$ and that at

that value K_{nom}/K_{crit} has a value greater than β. The very large and very small γ limits discussed in the body of the paper still apply here as shown in Eq. (IV.24) and Figure 6.

It should be pointed out here that the solution for all field variables due to the loading $\tau(x)$ is available by direct integration. That is, the results of (IV.15) can be applied to find a, b and d, (IV.6), which in turn determine $\tilde{f}$, the transform of any field variable, through (IV.3). These can be inverted with (IV.1b) and the general solution then found through superposition (IV.12). Though straightforward, these steps are quite (!) cumbersome and the results would ultimately depend on the numerical evaluation of a single or double integral. Fortunately, these calculations are not needed for the results we seek.

Though we have solved a portion of the full field equations, we have not checked explicitly any of the boundary conditions. Instead we put trust in our method of solution based on the fact that it works for a mathematically simpler limiting case discussed in the next section.

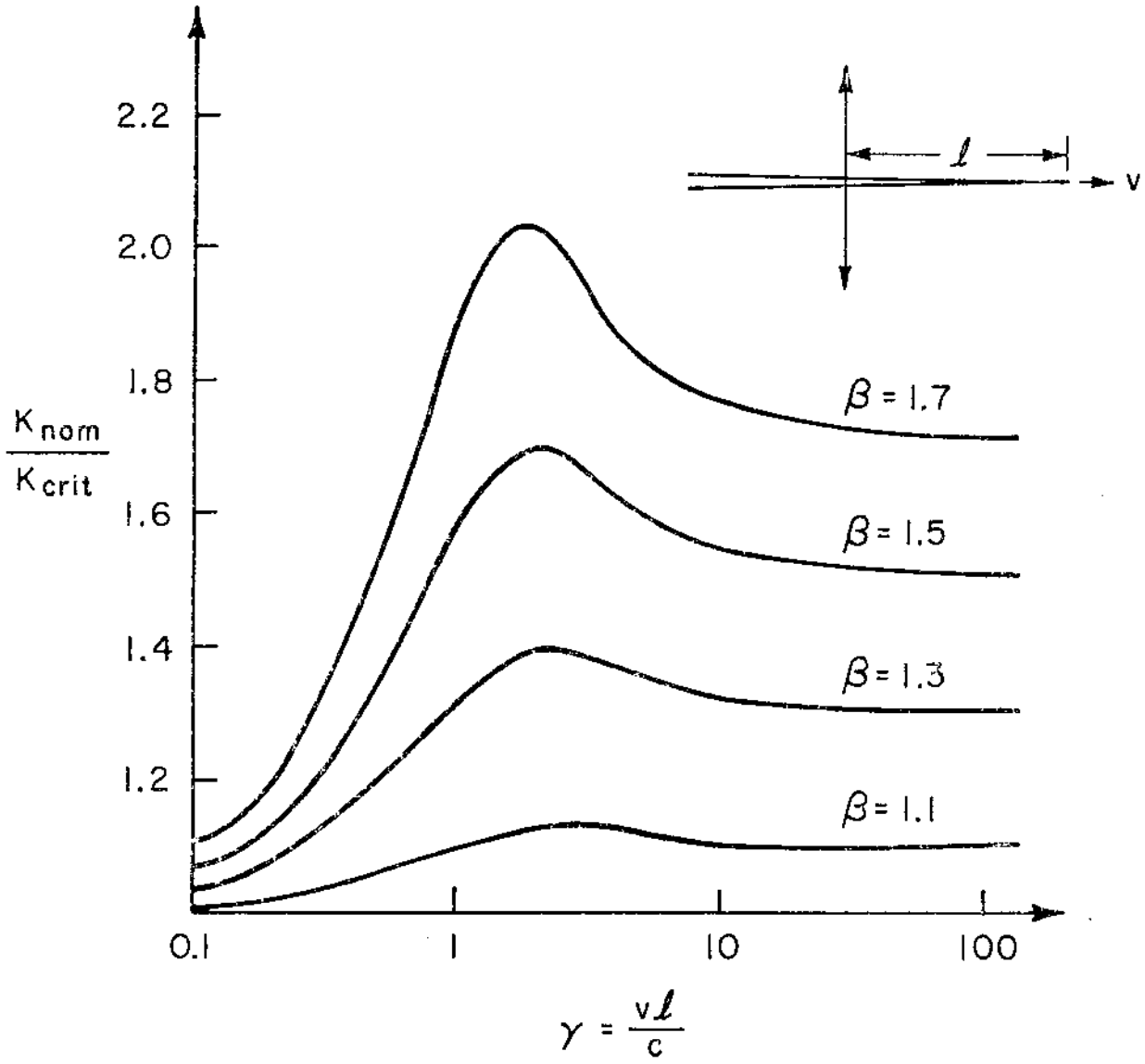

FIG. 6 INCREASE IN REQUIRED LOADS WITH INCREASING SPEED FOR A POINT LOAD A DISTANCE ℓ FROM THE CRACK TIP.

APPENDIX V

Asymptotic Boundary Condition

Before the transition from case II to case III can be discussed, the solution to the relevant field equations must be obtained.

In this case we have $\ell >> c/v$ and $\ell >> \omega$ (the relative size of ω and c/v does not matter at this point). Therefore, by previous arguments in the far field where $r >> c/v$ (but still $r << \ell$), stresses are dominated by the $r^{-1/2}$ terms of ordinary linear elasticity. In the range of $r \approx c/v$ the field is not known. The full coupled equations must be used, but the boundary conditions are simplified. The loading on the crack faces in the region $r \lesssim c/v$ has vanishing effect as $\ell v/c \to \infty$ (as in [18]). Instead, the near-tip region is effectively loaded by the distant $r^{-1/2}$ elastic field. The problem posed then is one for which there are no loads on the crack faces but the solution must asymptotically approach the far field $r^{-1/2}$ elastic solution.

The fourier transform and resulting equations follow as before through (IV.9), in which we now set $\tilde{\tau}(\kappa) = 0$ to give

$$\frac{G^+(\kappa)}{2(\mu-1)m^+(\kappa)} = \frac{F^-(\kappa)m^-(\kappa)}{D^-(\kappa)} \quad . \tag{V.1}$$

The stress field immediately at the crack tip was shown to have the standard $r^{-1/2}$ singularity. This, with the asymptotic boundary condition means that $\sigma_{yy}(x) = K_{nom}\, g(x)/\sqrt{2\pi x}$ where K_{nom} is the far field stress intensity factor and $g(x)$ is a bounded function that approaches 1 as $x \to \infty$. This has two useful consequences: 1) From the definition of F^-

the right side of (V.1) is bounded as $\kappa \to \infty$. 2) By direct calculation $F^-(\kappa)$ is asymptotically approximated by $(1-i)K_{nom}\kappa^{-1/2}/2$ as $\kappa \to 0$. Since the right side of (V.1) is bounded as $\kappa \to \infty$, the right side is a constant for all κ with negative imaginary part and the left side is the same constant for all κ with positive imaginary part (as argued before). The asymptotic form of $F^-(\kappa)$ and the limiting value $D^-(0) = 1$ are used to evaluate the constant from which it is found that

$$F^-(\kappa) = K_{nom}(1-i)D^-(\kappa)/(2m^-(\kappa)) \qquad (V.2a)$$

$$G^+(\kappa) = K_{nom}(\mu-1)(1-i)m^+(\kappa) \quad . \qquad (V.2b)$$

By using the fact that

$$\int_0^\infty x^{-1/2}e^{-ix}dx = \sqrt{\pi}(1-i)/\sqrt{2}$$

and the asymptotic forms of (V.2a) as $\kappa \to 0$ or ∞ , it can be seen that $F^-(\kappa)$ is the transform of a function $\sigma_{yy}(x,0)$ such that

$$\sigma_{yy}(x,0) \sim (1-\mu)K_{nom}/(2\pi x)^{1/2} \quad \text{as} \quad x \to 0 \qquad (V.3a)$$

$$\sigma_{yy}(x,0) \sim K_{nom}/(2\pi x)^{1/2} \quad \text{as} \quad x \to \infty \quad . \qquad (V.3b)$$

Equation (V.3b) is a verification of the boundary condition and (V.3a) is a duplicate of the result found in (IV.21b). In this case, however, the result applies to any crack face loading that is not singular at the crack tip and has a length scale large compared to c/v (unlike (IV.21b) which was found from the specific loading of Fig. (2b).).

Using the definitions of m , n , m^+ , m^- , n^- from (IV.4) and (IV.8),

the result of (V.2b) can be used to find the constants in (IV.6).

$$a(\kappa) = K_{nom}(1-i)/(2\bar{m}(\kappa))$$

$$b(\kappa) = -\mu K_{nom}(1-i)/(2\bar{n}(\kappa)) \qquad \text{(V.4)}$$

$$d(\kappa) = -c\mu K_{nom}(1+i)\bar{m}(\kappa)/v \quad .$$

These constants can be used in (IV.3) to give the full transforms of all field variables. These transforms can be inverted by the same general formula used by Simons [18] and found in Carrier, Crook and Pierson (1966), pg. 93. For our purposes, this equation can be written as

$$\text{if} \quad \tilde{G}(\kappa,y) = \frac{1}{(\kappa-ik)^{1/2}} e^{-y[(\kappa+ia)(\kappa-ik)]^{1/2}} \qquad \text{(V.5a)}$$

$$\text{then} \quad G(x,y) = \frac{(1+i)}{\sqrt{2\pi r}} e^{-r(a+k)/2 + x(a-k)/2} \cos(\theta/2)$$

$$\text{and if} \quad \tilde{G}(\kappa,y) = \frac{1}{(\kappa+ik)^{1/2}} e^{-y[(\kappa-ia)(\kappa+ik)]^{1/2}} \qquad \text{(V.5b)}$$

$$\text{then} \quad G(x,y) = \frac{1-i}{\sqrt{2\pi r}} e^{-[(a+k)r+(a-k)x)/2} \sin(\theta/2)$$

$$\text{for} \quad a,K,y > 0 \quad .$$

These two transform formulas are used extensively in the calculations that follow, as are the following two rules about the derivatives of a field variable whose transform $\tilde{G}$ has the form $\tilde{G} = f(\kappa)e^{-g(\kappa)y}$:

$$\text{transf.}\left\{\frac{\partial}{\partial x}G(x,y)\right\} = i\kappa\tilde{G}(\kappa,y) \tag{V.6a}$$

$$\text{transf.}\left\{\frac{\partial}{\partial y}G(x,y)\right\} = -g(\kappa)\tilde{G}(\kappa,y) \quad . \tag{V.6b}$$

While deriving (IV.3), it was found that the variables solving the field equations (I.9) and (I.12) have transforms given by:

$$\tilde{\sigma}_{xx} + \tilde{\sigma}_{yy} + 2\eta\tilde{p} = 2(1-\mu)a(\kappa)e^{-m(\kappa)y} \tag{V.7a}$$

$$\tilde{\sigma}_{xx} + \tilde{\sigma}_{yy} + (2\eta/\mu)\tilde{p} = -[(1-\mu)/\mu]b(\kappa)e^{-n(\kappa)y} \quad . \tag{V.7b}$$

By using (V.5a) with the definitions of $m(\kappa)$ and $n(\kappa)$, both of (V.6) can be inverted directly to give

$$\sigma_{xx} + \sigma_{yy} + 2\eta p = 2\,\frac{K_{nom}}{\beta\sqrt{2\pi r}}\cos(\theta/2) \tag{V.8a}$$

$$\sigma_{xx} + \sigma_{yy} + (2\eta/\mu)p = 2\,\frac{K_{nom}}{\beta\sqrt{2\pi r}}\,e^{-v(r+x)/(2c)}\cos(\theta/2) \quad . \tag{V.8b}$$

Equations (V.8) can be solved for the mean normal stress and pore pressure to give

$$(\sigma_{xx} + \sigma_{yy})/2 = \frac{K_{nom}}{\sqrt{2\pi r}}\left(1 - \mu e^{-vr(1+\cos\theta)/(2c)}\right)\cos(\theta/2) \tag{V.9a}$$

$$p = \frac{-K_{nom}}{\sqrt{2\pi r}}\;\frac{2B(1+\nu_u)}{3}\left(1 - e^{-vr(1+\cos\theta)/2c}\right)\cos(\theta/2) \quad . \tag{V.9b}$$

Also, while deriving (IV.3), it was found that

$$(\tilde{\sigma}_{yy} - \tilde{\sigma}_{xx})/2 = (d+mya)e^{-my} + \left(\frac{\kappa^2+n^2}{\kappa^2-n^2}\right)be^{-ny} \quad . \tag{V.10}$$

With some manipulation and use of (V.5), this becomes

$$\frac{(\sigma_{yy}-\sigma_{xx})}{2} = \frac{-2c\mu K_{nom}}{v}\frac{\partial}{\partial x}\left\{\frac{\cos(\theta/2)}{\sqrt{2\pi r}}\left[1-\frac{1}{2}e^{-vr(1+\cos\theta)/(2c)}\right]\right\}$$

$$-K_{nom}\left\{y\frac{\partial}{\partial y}\left[\frac{\cos(\theta/2)}{\sqrt{2\pi r}}\right]+\frac{c\mu}{v}\frac{\partial}{\partial y}\left[\frac{\sin(\theta/2)}{\sqrt{2\pi r}}e^{-vr(1+\cos\theta)/(2c)}\right]\right\}. \tag{V.11}$$

The inverse transform of σ_{xy} can also be found from (IV.3c) to be

$$\sigma_{xy} = \frac{\mu c K_{nom}}{v}\left\{2\frac{\partial}{\partial x}\left[\frac{\sin(\theta/2)}{\sqrt{2\pi r}}\right]-\frac{vy}{\mu c}\frac{\partial}{\partial x}\left[\frac{\cos(\theta/2)}{\sqrt{2\pi r}}\right]\right.$$

$$\left.-2\frac{\partial}{\partial y}\left[\frac{e^{-r(1+\cos\theta)v/(2c)}}{\sqrt{2\pi r}}\cos(\theta/2)\right]\right\}. \tag{V.12}$$

Equations (V.9), (V.11) and (V.12) are the solution to the field equations for $v\ell/c >> 1$ and $x << \ell$. They can be solved for σ_{xx}, σ_{yy}, σ_{xy} and p. The resulting calculation is cumbersome and is thus only carried out on the x axis for σ_{xy}, σ_{xx}, σ_{yy} and p and on the y axis for σ_{xy}. The solution then takes the form

$$\sigma_{xy}(x,0) = 0 \tag{V.13a}$$

$$p(x,0) = \frac{-K_{nom}}{\sqrt{2\pi x}}\frac{2B(1+\nu_u)}{3}\left[1-e^{-vx/c}\right], \quad (x>0) \tag{V.13b}$$

$$\sigma_{xx}(x,0) = \frac{K_{nom}}{\sqrt{2\pi x}}\left\{1-\frac{c\mu}{vx}\left[1-e^{-vx/c}\right]\right\}, \quad (x>0) \tag{V.13c}$$

$$\sigma_{yy}(x,0) = \frac{K_{nom}}{\sqrt{2\pi x}} \left\{ 1 - \mu \left[2e^{-vx/c} - \frac{c}{vx} (1-e^{-vx/c}) \right] \right\} , \quad (x>0) \quad ,$$

(V.13d)

$$\sigma_{yy}(x,0) = \sigma_{xx}(x,0) = p(x,0) = 0 \quad , \quad (x<0) \qquad \text{(V.13e)}$$

$$\sigma_{xy}(0,y) = \frac{-K_{nom}}{2\sqrt{2}\sqrt{2\pi x}} \left\{ 1 - \mu \left[2e^{-yv/2c} - \frac{2c}{yv} (1-e^{-yv/2c}) \right] \right\} \quad . \qquad \text{(V.13f)}$$

A few features of the solution may be pointed out here. Firstly, the functions satisfy the boundary conditions and asymptotically approach the expected elastic fields as $r \to 0$ and $r \to \infty$. This is not immediately apparent in (V.11) and (V.12), but can be seen clearly in (V.9b) and (V.13) by comparing with the field predicted for an ordinary elastic body [19]. Secondly, (V.9b) and (V.13e) show that the pore pressure is zero on the crack faces. Thus the equations satisfy a zero pore pressure boundary condition on the negative x-axis. In a model of hydraulic fracture, this fact is perhaps of little significance. It is interesting to note for other applications that the solution satisfies two different boundary conditions — both no pore fluid flow through the crack faces and zero pore pressure on the crack faces.

Since the concept of drained and undrained behavior is used often in porous media discussions, it is interesting to check the degree of "drainedness" at each point in the body; call it Δ (similar to a parameter used in Simons [18]) and define $\Delta \equiv p/p_u$,

$$p_u \equiv \frac{-2B(1+\nu_u)}{3} \frac{\sigma_{xx}+\sigma_{yy}}{2}$$

is the pore pressure the stresses would imply if the medium were totally undrained. Use of (V.9b) shows that lines of constant Δ are parabolas opening around the negative x-axis with foci at the origin. This is the same result obtained in Simons [18] for the shear fault.

Transition from Case II to Case III

Here we have $c/v >> \ell$ and we examine the transition as ω goes from much smaller to much larger than c/v with increasing v. The criterion used for crack propagation is that the Terzaghi effective stress, $\bar{\sigma} \equiv \sigma + p$ reach a level of $\bar{\sigma}_{crit}$ at a distance ω ahead of the crack tip. This criterion is expressed by the relation $\bar{\sigma}(\omega) = \bar{\sigma}_{crit}$. Using (V.13b) and (V.13d), this becomes

$$\bar{\sigma}(\omega) = \bar{\sigma}_{crit} = \frac{K_{nom}}{\sqrt{2\pi\omega}} \left\{ 1 - \frac{\nu_u - \nu}{1-\nu} \left[2e^{-v\omega/c} - \frac{c}{v\omega} (1-e^{-v\omega/c}) \right] - \frac{2B(1+\nu_u)}{3} \left| 1-e^{-v\omega/c} \right| \right\} \tag{V.14}$$

Of interest is how much greater K_{nom} in (V.14) is than the K_{crit} required for the same fracture criterion in a totally elastic body; i.e.,

$$\frac{K_{crit}}{\sqrt{2\pi\omega}} = \bar{\sigma}_{crit} \quad .$$

The sought effect is then included in the equation which follows from (V.14):

$$\frac{K_{nom}}{K_{crit}} = \left\{ 1 - \frac{\nu_u - \nu}{1-\nu} \left[2e^{-v\omega/c} - \frac{c}{v\omega} (1-e^{-v\omega/c}) \right] - \frac{2B(1+\nu_u)}{3} (1-e^{-v\omega/c}) \right\}^{-1} . \tag{V.15}$$

The form of the function (V.15) is such that the general shape of the K_{nom}/K_{crit} vs. v curve is unaffected by the other parameters in the equation.

Figure 4 illustrates the effect for a few values of material constants (constants chosen from Rice and Cleary [12]).

APPENDIX VI

Application to Unsteady Crack Growth

One may expect the solution for constant v to be applicable, at least approximately, to unsteady v in some circumstances. For example, if f is a field variable its value is a functional of the full history of crack tip motion in addition to the position of the point at some current time t. One might assume this functional can be simplified to $f = f(x,y,v,\dot{v},\ddot{v},\dddot{v} \ldots)$ where x and y are coordinates relative to the crack tip. The incremental change of f at a material point would then be

$$df = [(\partial f/\partial x)v + (\partial f/\partial v)\dot{v} + \ldots]dt \ .$$

Neglecting terms from $\ddot{v}$ on, one is left with an expression for which all terms can be calculated from the general steady state solution:

$$df = \left[(\partial f/\partial x)v + (\partial f/\partial v)\dot{v}\right]dt \ .$$

If however, $|(\partial f/\partial x)v| >> |\partial f/\partial v)\dot{v}|$ then $df \approx -(\partial f/\partial x)\dot{v}dt$ which is exactly the value of df that the steady state solution implies. This condition should prevail near the crack tip where spatial gradiants $(\partial f/\partial x)$ are very high.